

Generalized Gouy Rotation of Electron Vortex beams in uniform magnetic fields

Qi Meng,¹ Xuan Liu,¹ Wei Ma,¹ Zhen Yang,¹ Liang Lu,^{1,2}
Alexander J. Silenko,³ Pengming Zhang,⁴ and Liping Zou^{1,*}

¹*Sino-French Institute of Nuclear Engineering and Technology, Sun Yat-Sen University, Zhuhai 519082, China*

²*United Laboratory of Frontier Radiotherapy Technology of Sun Yat-sen University &
Chinese Academy of Sciences Ion Medical Technology Co., Ltd., Guangzhou 510000, China*

³*Bogoliubov Laboratory of Theoretical Physics, Joint Institute for Nuclear Research, Dubna 141980, Russia*

⁴*School of Physics and Astronomy, Sun Yat-sen University, Zhuhai 519082, China*

The rotation of electron vortex beams (EVBs) presents a complex interplay of the Gouy phase characterizing free-space behavior and Landau states or Larmor rotation observed in magnetic fields. Despite being studied separately, these phenomena manifest within a single beam during its propagation in magnetic fields, lacking a comprehensive description. We address this by utilizing exact solutions of the relativistic paraxial equation in magnetic fields, termed “paraxial Landau modes”. The paraxial Landau modes describe the quantum states of EVBs in magnetic fields. Our study of rotation angles demonstrates consistency with experimental data, supporting the practical presence of these modes. We provide a unified description of different regimes under generalized Gouy rotation, linking the Gouy phase to EVB rotation angles. This connection enhances our understanding of the Gouy phase and can be extended to nonuniform magnetic fields. Our theoretical analysis is validated through numerical simulations using the Chebyshev method. This work offers new insights into the dynamics of EVBs in magnetic fields and suggests practical applications in beam manipulation and beam optics of vortex particles.

Introduction. — Vortex beams, characterized by their quantized orbital angular momentum (OAM) along the axis of propagation and helical wavefronts, represent a powerful tool endowed with an additional degree of freedom for exploring new physics [1–4]. Researches on vortex beams have advanced across multiple disciplines, including particle physics [5–10], optics [11–14], nuclear physics [15–17], atomic and molecular physics [18–20], condensed matter physics [21–23], and astrophysics [24], among others. Within this broad range, vortex electrons have been extensively investigated [25–32]. Specifically, consistent efforts are directed towards understanding their behaviors in magnetic fields [3–6, 33–40] and one widely discussed topic is the rotational dynamics of EVBs [3–6].

Understanding the rotational dynamics of EVBs in magnetic fields, particularly in the context of transmission electron microscopy (TEM), presents a complex challenge both experimentally and theoretically. Visualizing the internal rotational dynamics of EVBs requires breaking the cylindrical symmetry, a task addressed in several experiments by partially cutting the beams [4–6]. These experiments reveal the quantized rotation of EVBs, dependent on topological charges and manifesting as Landau states [3], while also observing the Gouy rotation near the focus and Larmor rotation at greater distances [5]. Remarkably, these rotational regimes have all been observed within a single beam at varying propagation distances [6]. This implies that current theoretical descriptions may not offer a comprehensive account of the phenomenon. A re-evaluation of the rotational dynamics is thus needed to integrate these observations into a cohesive framework.

The relativistic paraxial equation in magnetic fields for electron beams can be derived from the Foldy-Wouthuysen (FW) Hamiltonian [35, 41]. The FW representation [42] establishes a Schrödinger picture of relativistic quantum mechanics [42, 43]. The exact solution of this equation proves to be a promising candidate for investigating EVBs in magnetic fields [35, 44], referring hereafter as “paraxial Landau modes”. The Landau states, commonly used to characterize electrons in uniform magnetic fields, emerge as special cases when the beam waist of paraxial Landau modes equals a magnetic length parameter [45]. Furthermore, as magnetic fields approach zero, the paraxial Landau modes transform into the free-space Laguerre-Gaussian (LG) beams [1].

Paraxial Landau modes exhibit a noteworthy characteristic of periodic oscillation in beam widths, which stands in contrast to the diffracting free LG beams or Landau electrons with constant beam width [35, 44, 46]. This behavior finds similarity with the optics domain, where similar periodic oscillations are observed in the propagation of LG beams through parabolic mediums [47, 48].

In free space, the Gouy phase [49–55] is associated with the rotational dynamics of EVBs [5]. However, the original form of Gouy rotation inadequately describes rotation within magnetic fields. The Gouy phase of the paraxial Landau modes takes on a distinct form compared to the familiar Gouy phase of free-space LG beams. This leads to a generalized Gouy rotation associated with paraxial Landau modes, which proves useful in describing rotational dynamics of EVBs in uniform magnetic fields.

In this Letter, we unify the various rotational regimes that manifest during the propagation of EVBs in a uni-

form magnetic field. The rotation angles of EVBs are theoretically calculated based on paraxial Landau modes, demonstrating consistency with the experimental data in [6]. To validate our findings, we conduct numerical simulations using the Chebyshev method. The resulting intensity profiles confirm our theoretical predictions regarding rotation angles. In our discussions, we differentiate our analytical single-mode analysis from an alternative method proposed in [6], which involves representing beams in magnetic fields as superpositions of free LG beams. We emphasize that our method considers not only converging EVBs but also incorporates the oscillating behavior of beam width induced by magnetic fields, thereby enhancing its applicability in electron optics.

Paraxial Landau modes.— The FW Hamiltonian is $\hat{H}_{\text{FW}} = \beta\sqrt{m^2c^4 + \hat{\pi}^2c^2} - e\hbar c^2\boldsymbol{\Sigma} \cdot \mathbf{B}$ [35, 41, 56], where $\hat{\pi} = \hat{p} - e\hat{\mathbf{A}}$ represents the kinetic momentum, $\hat{\mathbf{A}} = \hat{\mathbf{B}} \times \hat{\mathbf{r}}/2$ is the vector potential in symmetric gauge, β and $\boldsymbol{\Sigma}$ are the Dirac matrices. The z axis of cylindrical coordinates (r, ϕ, z) is directed along magnetic field, $\mathbf{B} = B\hat{z}$. The electron charge is $e = -|e|$. The spin term $s_z B$ can be disregarded because it can be eliminated together with m^2 after the zero energy level shift [35]. Using the paraxial approximation $\hat{\pi}^2 \approx p\hat{p}_z + \hat{\pi}_\perp^2/2$ together with ansatz $\psi = e^{ikz}\Psi$, one can obtain the paraxial equation for EVBs in uniform magnetic fields [35]:

$$\left[2i\hbar^2k \frac{\partial}{\partial z} + \hbar^2\nabla_\perp^2 - i\hbar eB \frac{\partial}{\partial \phi} - \frac{1}{4}e^2B^2r^2 \right] \Psi = 0, \quad (1)$$

where k is the wave number related to momentum by the de Broglie relation $p = \hbar k$, and p satisfies the relativistic dispersion relation $E^2 = m^2c^4 + p^2c^2$. ∇_\perp^2 is the transverse Laplace operator in cylindrical coordinates. The *exact* form of Eq. (1) has been obtained in [41]. For $B = 0$, this equation becomes the paraxial equation in free space [1].

The exact solution of the paraxial equation (1) is [35, 44, 46, 57]

$$\Psi_{n\ell} = A e^{i(\ell\phi + \frac{kr^2}{2R(z)} - \Phi_G(z))}, \quad (2a)$$

$$A = \frac{C_{n\ell}}{w(z)} \left(\frac{\sqrt{2}r}{w(z)} \right)^{|\ell|} L_n^{|\ell|} \left(\frac{2r^2}{w(z)^2} \right) e^{-\frac{r^2}{w(z)^2}}, \quad (2b)$$

$$C_{n\ell} = \sqrt{\frac{2n!}{\pi(n+|\ell|)!}}, \quad (2c)$$

The real function A defines the amplitude. $L_n^{|\ell|}$ is the generalized Laguerre polynomial, with $n = 0, 1, 2, \dots$ the radial quantum number and $\ell = 0, \pm 1, \pm 2, \dots$ the topological charge. $w(z)$ is the beam width, $R(z)$ is the radius of curvature of the wavefront, and $\Phi_G(z)$ is the

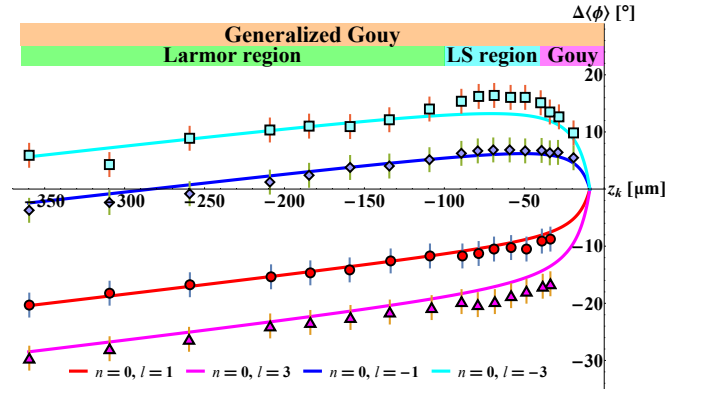


FIG. 1. The calculated rotation angles $\Delta\langle\phi\rangle$ as functions of knife-edge positions z_k . The cyan squares, the blue rhombus, the red circles, and the magenta triangles represent the experimental data for EVBs with $\ell = -3, -1, 1, 3$, respectively. The solid lines represent our theoretical analysis, where we use the colors cyan, blue, red, and magenta as for experimental data. The Rayleigh distances used in the experiment are $z_R = 1.46 \mu\text{m}$ for $|\ell| = 1$ and $z_R = 2.84 \mu\text{m}$ for $|\ell| = 3$; the observation plane is shifted from the focus plane by a distance $z_{af} = -9 \mu\text{m}$. Note that $\Delta\langle\phi\rangle$ is plotted in degree, requiring an additional factor of $180/\pi$ in Eq. (6).

Gouy phase:

$$w(z) = w_0 \sqrt{\cos^2 \frac{z}{z_m} + \frac{z_m^2}{z_R^2} \sin^2 \frac{z}{z_m}}, \quad (3a)$$

$$R(z) = kw_m^2 \frac{\cos^2 \frac{z}{z_m} + \frac{z_m^2}{z_R^2} \sin^2 \frac{z}{z_m}}{\left(\frac{z_m^2}{z_R^2} - 1 \right) \sin \frac{2z}{z_m}}, \quad (3b)$$

$$\Phi_G(z) = N \arctan \left(\frac{z_m}{z_R} \tan \frac{z}{z_m} \right) + \ell \frac{z}{z_m}, \quad (3c)$$

where $N = 2n + |\ell| + 1$, w_0 is the beam waist, $z_R = kw_0^2/2$ is the Rayleigh distance, $w_m = 2\sqrt{\hbar}/|e|B$ is a magnetic length parameter, and $z_m = kw_m^2/2$ is related to the Larmor distance through $z_L = 2\pi z_m$ [4]. When taking the limit $B \rightarrow 0$, the parameter functions in Eq. (3) become that of free-space LG beams [35] and if the condition $w_m = w_0$ is satisfied, Landau states are recovered [45] (except for the additional Gouy phase coming from the paraxial approximation). Note that the beam width given by Eq. (3a) oscillates with a spatial period of πz_m . This oscillation implies the emergence of multiple foci along the beam propagation path.

Rotational Dynamics.— The rotation of EVBs in magnetic field is closely linked to Bohmian trajectories [1, 4, 6]. These trajectories illustrate the spiralling motion of electrons around the direction of magnetic fields. When considering the presence of a vector potential \mathbf{A} , the gauge-invariant probability current is [1, 58]: $\mathbf{j} = [\hbar \text{Im}(\psi^* \nabla \psi) - e\mathbf{A}|\psi|^2]/m$. The angular velocity of electron is related to the current through: $\omega(r) = v_\phi(r)/r = \hbar\ell/mr^2 + \omega_L$ (where $\rho = |\psi|^2$, $\mathbf{v} = \mathbf{j}/\rho$ is the

local Bohmian velocity, and $\omega_L = |e|B/2m$ is the Larmor frequency). Its expectation value turns out to be

$$\langle \omega \rangle (z) = \omega_L \left(\text{sgn}(\ell) \frac{w_m^2}{w(z)^2} + 1 \right), \quad (4)$$

where we have used the fact that for $\ell \neq 0$, $\langle r^{-2} \rangle = 2/|\ell|w(z)^2$ [6, 59]. For Landau states, $w(z) = w_m$ and we recover the quantized rotation of Landau electrons: $\langle \omega \rangle (z) = \omega_L (\text{sgn}(\ell) + 1)$ [3, 4]. Depending on the sign of topological charge ℓ , it can take values of cyclotron frequency $\omega_c = 2\omega_L$, Larmor frequency ω_L , and zero.

Changing the time increment to experimentally accessible z -shift $\langle \omega \rangle = d\langle \phi \rangle / dt = v d\langle \phi \rangle / dz$, we can then calculate the Bohmian rotation angle through $\langle \phi \rangle = \int \langle \omega \rangle dz / v$:

$$\langle \phi \rangle = \text{sgn}(\ell) \arctan \left(\frac{z_m}{z_R} \tan \left(\frac{z}{z_m} \right) \right) + \frac{z}{z_m}. \quad (5)$$

The first term in Eq. (5) can be seen as the reminiscent of free-space Gouy rotation, dominant near the focus. Meanwhile, the second term z/z_m arises from the Zeeman coupling of electron OAM with magnetic field and

represents Larmor rotation, dominant far from the focus. In the limited region where both effects are comparable, the so-called ‘‘LS’’ (Landau states) region with quantized rotation manifests.

An important observation of this letter is that $\langle \phi \rangle$ exactly corresponds to the part with coefficient ℓ in the Gouy phase of paraxial Landau modes, as described in Eq. (3c). This generalizes the concept of Gouy rotation from free space to magnetic fields. These rotation regimes are shown and marked with different colors in Fig. 1.

The formula (5) for rotation angles can be related to the experimental data in [6]. In the experiment, an incident electron beam is initially transformed into EVBs using a holographic fork mask. The EVBs then encounter a longitudinal magnetic field produced by the objective lens of TEM. The EVBs continue to propagate until they reach a knife-edge (KE). Subsequently, the cut EVBs proceed along the column, ultimately reaching the observation plane positioned above focal plane, i.e. the defocus position z_{df} . The rotational dynamics of the EVBs are studied by adjusting the position of KE z_k , resulting in variations in azimuthal angles of the half-moon-like patterns on observation plane:

$$\Delta \langle \phi \rangle = \text{sgn}(\ell) \left[\arctan \left(\frac{z_m}{z_R} \tan \left(\frac{z_k}{z_m} \right) \right) - \arctan \left(\frac{z_m}{z_R} \tan \left(\frac{z_{df}}{z_m} \right) \right) \right] + \frac{z_k - z_{df}}{z_m}. \quad (6)$$

It is worth mentioning that the transmission of twisted electrons through sharp boundary between vacuum and solenoid is addressed recently [46], which enables the smooth transition of free LG beams to paraxial Landau modes in magnetic fields. Additionally, it should be noted that the arc tangent term in Eq. (6) is understood hereafter as $\left(\arctan \left(\frac{z_m}{z_R} \tan \frac{z}{z_m} \right) + \pi \left[\frac{z}{\pi z_m} + \frac{1}{2} \right] \right)$ to ensure its continuity over $(-\infty, \infty)$, where $[\cdot]$ denotes the floor function [44].

In the experiment [6], the magnetic field used is $B = 1.9$ T for a standard TEM objective lens. Under the working energy of 200 keV, the electron travels at a relativistic speed $v \simeq 0.7c$, where c is the speed of light. The relativistic mass of the electron is $m = \gamma m_0$, where m_0 denotes the rest electron mass. Utilizing $w_m = 2\sqrt{\hbar}/|e|B$ and the wave number $k = mv/\hbar$, we can determine the characteristic distance: $z_m = kw_m^2/2 \simeq 1768 \mu\text{m}$.

The theoretical analysis based on Eq. (6) is plotted in Fig. 1 for EVBs with different topological charges $\ell = \pm 1, \pm 3$, which are consistent with the experimental data. In the experimental conditions utilized here, the Gouy rotation exhibits notably rapid behavior near the focal point. Importantly, in the region ranging from

$-80 \mu\text{m}$ to $-30 \mu\text{m}$, we have the approximate Landau states characterized by $w(z) \simeq w_m$, in agreement with the experiment in [4]. The experiment in [5] made separate observations of the Gouy rotation in free space and Larmor rotation in magnetic fields, whereas in our context both are observed in magnetic fields. They can be considered as components of the generalized Gouy rotation that dominate across different ranges.

Simulations.— To further validate our theoretical analysis and enable subsequent discussions, we perform numerical simulations using the paraxial equation (1) as the governing equation. The simulations are initialized with the truncated paraxial Landau modes, described by

$$\Phi(\mathbf{r})|_{z=z_k} = \begin{cases} \Psi_{n\ell}(\mathbf{r})|_{z=z_k}, & \phi \in (0, \pi) \\ 0, & \phi \in (\pi, 2\pi). \end{cases} \quad (7)$$

It is worth noting that the truncated beam Φ represents a superposition of numerous paraxial Landau modes, which interfere and result in complex diffraction deformations [5]. Its OAM expectation value proves to be approximately conserved, $\langle \hat{L}_z \rangle \approx \hbar \ell$ [5, 6].

The numerical method used here is the Chebyshev method. Although it is originally applied to solve the time-dependent Schrödinger equation (TDSE) [37, 60],

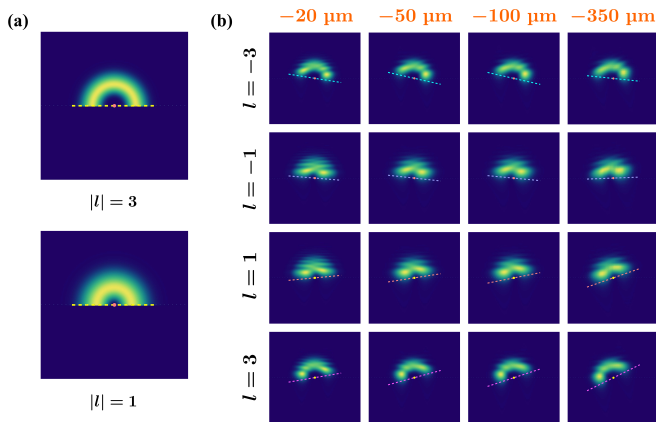


FIG. 2. (a) The initial intensity profiles of Φ on the KE plane as reference. (b) The simulated intensity profiles of Φ on the observation plane for EVBs with radial index $n = 0$ and topological charge $\ell = -3, -1, 1, 3$ respectively, at four distinct cutting positions: $z_k = -20 \mu\text{m}, -50 \mu\text{m}, -100 \mu\text{m}, -350 \mu\text{m}$. The dashed lines overlaid on the intensity profiles indicate the opposite of theoretically calculated angles described in Eq. (6) since we are comparing the intensity profiles at the observation plane with the KE plane. Remarkably, these lines are in accordance with the observed rotation angles of the intensity profiles.

we notice that Eq. (1) can be transformed to a TDSE-like form:

$$i\hbar \frac{\partial}{\partial z} \Phi = \left[-\frac{\hbar}{2k} \nabla_{\perp}^2 + i \frac{eB}{2k} \frac{\partial}{\partial \phi} + \frac{e^2 B^2 r^2}{8\hbar k} \right] \Phi. \quad (8)$$

The transverse scales vary significantly from the smallest z -shift to the observation plane: $(w(-350 \mu\text{m})/w(-9 \mu\text{m}))^2 \simeq 1600$. To ensure stability and precision in the simulation, a fine spatial grid is necessary. In this context, the Chebyshev method is appropriate. Acting as a global approximation technique, it facilitates the direct calculation of the final states once the Hamiltonian and initial states of the system are provided. This is achieved by expanding the unitary propagation operator as a series of Chebyshev polynomials, as discussed in [37, 60].

The simulated results are shown in Fig. 2. The rotations of half-moon-like intensity profiles can be seen to match the dashed lines representing our theoretical analysis in Eq. (6). Specifically, at $z_k = -20 \mu\text{m}$ and $-50 \mu\text{m}$, the intensity profiles exhibit rapid Gouy rotation. Subsequently, from $-50 \mu\text{m}$ to $-80 \mu\text{m}$, the intensity profiles for $\ell < 0$ undergo minimal rotation, indicative of the zero frequency associated with the Landau states. Noteworthy observations emerge from $-100 \mu\text{m}$ to $-350 \mu\text{m}$. EVBs with positive ℓ values exhibit consistent rotation in one direction, while those with negative ℓ values demonstrate a reversal of rotation, as can be observed in Fig. 2 (b).

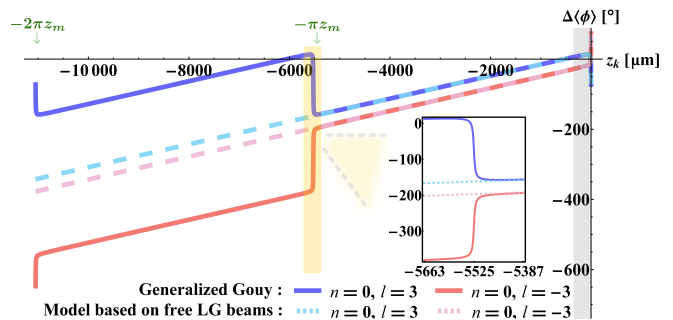


FIG. 3. Rotation angles $\Delta\langle\phi\rangle$ as functions of z_k for generalized Gouy rotation and model based on free LG beams. We use the Rayleigh distance $z_R = 2.84 \mu\text{m}$ for $n = 0, |\ell| = 3$ as in the experiment and extends the z -shift range down to $-2\pi z_m$ for differentiation between the two approaches. The gray band represents the accessed z -shift range in the experiment. The region near the focus at $-\pi z_m$ is magnified to illustrate the fast yet continuous Gouy rotation.

Discussions.— Our method using analytical solutions is different from that used in [6]. The latter involves decomposing the wave function in magnetic fields into free LG beams. It is noted that for converging EVBs in magnetic fields with vortex order ℓ , free LG beams of the same order ℓ provide a viable approximation, while those of different orders serve as minor admixtures. By substituting the beam width $w(z) = w_0 \sqrt{1 + z^2/z_R^2}$ of free LG beams into Eq. (4), one can derive a formula for the rotation angles:

$$\Delta\langle\phi\rangle = \text{sgn}(\ell) \left[\arctan\left(\frac{z_k}{z_R}\right) - \arctan\left(\frac{z_{df}}{z_R}\right) \right] + \frac{z_k - z_{df}}{z_m}. \quad (9)$$

In the range of accessible z -shifts and under the parameters employed in the experiment, the model based on free LG beams also demonstrates agreement with the experimental data [6]. This is attributed to its effectiveness in describing converging EVBs. Within the explored experimental range, the beam maintains its convergent characteristics.

Our method takes into account the oscillating behavior of beam width induced by magnetic fields. One can extend the range of z -shifts such that the beam demonstrates both divergent and convergent behaviors and the result is shown in Fig. 3. Nevertheless, simulating within extended range under the original experimental parameters presents challenges due to a significant variation in transverse scales, characterized by $(w(-\pi z_m/2)/w(z_{df}))^2 \simeq 35000$. To further distinguish between the two approaches and facilitate simulations, we opt for a Rayleigh distance of $z_R = 1000 \mu\text{m}$. This amounts to choosing a beam waist of approximately 20 nm rather than the 1 nm used in the experiment, which has demonstrated its feasibility in [5]. The results are shown in Fig. 4 and it should be noticed that

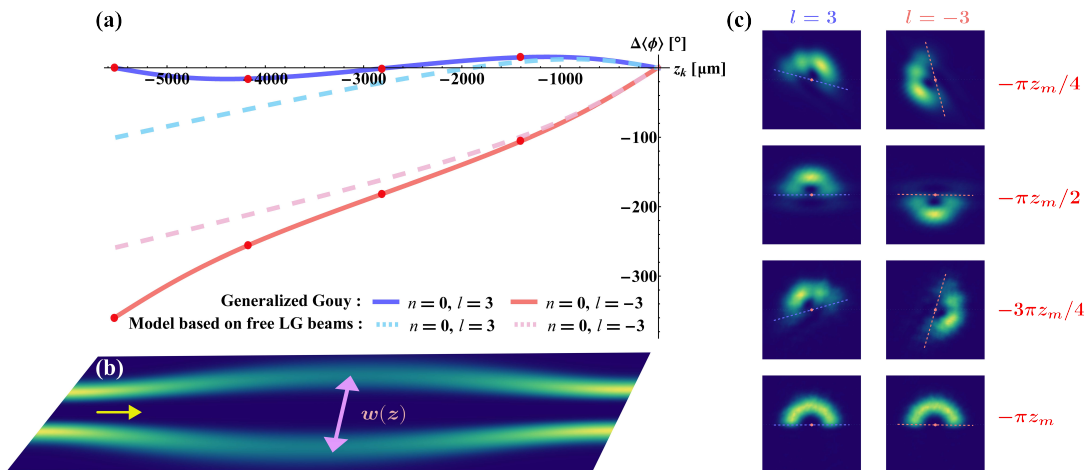


FIG. 4. (a) Rotation angles $\Delta\langle\phi\rangle$ as functions of z_k for generalized Gouy rotation and model based on free LG beams. The Rayleigh distance used here is $z_R = 1000 \mu\text{m}$, in contrast to the experimental value of $2.84 \mu\text{m}$ for $n = 0, |\ell| = 3$. The red points indicate the locations where simulations are conducted. (b) The longitudinal slice of the beam intensity profile illustrates the change in beam width $w(z)$, indicating beam undergoes both divergence and convergence along its propagation. The yellow arrow indicates the direction of beam propagation. (c) The simulated intensity profiles for $n = 0, |\ell| = 3$ at different cutting positions $z_k = -\pi z_m/4, -\pi z_m/2, -3\pi z_m/4, -\pi z_m$. The dashed lines represent the theoretical predictions based on Eq. (6), which are consistent with simulations.

for $z_k \leq -\pi z_m/2$ the beam undergo divergence and the difference becomes apparent.

Further experiment verifications could involve employing a low-energy TEM [61, 62], or increasing the magnetic field. Both strategies aim to reduce $z_m = 2mv/|e|B$ such that the critical position $-\pi z_m$ lies within the accessible region of the experiment, as depicted in Fig. 3.

Conclusions.— The rotational dynamics of EVBs in uniform magnetic fields is investigated based on the exact solution of the relativistic paraxial equation termed “paraxial Landau modes”. Our theoretical analysis, in alignment with experimental data and numerical simulations, supports the practical presence of paraxial Landau modes. We unveil the connection between the Gouy phase of paraxial Landau modes and rotation angles of EVBs and unify different rotational regimes under the generalized Gouy rotation which may extend to nonuniform magnetic fields (e.g., Glaser fields). The Chebyshev method is applied to numerically solve paraxial equations and simulate beam rotations. By measuring the rotation angles of EVBs in magnetic fields, spatially resolved measurements of longitudinal magnetic field components can be achieved. Our findings not only contribute to the fundamental understanding of the dynamics of EVBs in magnetic fields but also hold potential for practical applications in beam manipulation and beam optics of vortex particles.

Acknowledgement.— The work was supported by the National Natural Science Foundation of China (grants No. 12175320 and No. 12375084) and Guangdong Basic and Applied Basic Research Foundation (grants No. 2022A1515010280 and No. 2022B1515120027).

* zoulp5@mail.sysu.edu.cn

- [1] K. Bliokh, I. Ivanov, G. Guzzinati, L. Clark, R. Van Boxem, A. B  ch  , R. Juchtmans, M. Alonso, P. Schattschneider, F. Nori, and J. Verbeeck, *Phys. Rep.* **690**, 1 (2017).
- [2] I. P. Ivanov, *Prog. Part. Nucl. Phys.* **127**, 103987 (2022).
- [3] K. Y. Bliokh, P. Schattschneider, J. Verbeeck, and F. Nori, *Phys. Rev. X* **2**, 041011 (2012).
- [4] P. Schattschneider, T. Schachinger, M. St  ger-Pollach, S. L  ffler, A. Steiger-Thirsfeld, K. Y. Bliokh, and F. Nori, *Nat. Commun.* **5**, 4586 (2014).
- [5] G. Guzzinati, P. Schattschneider, K. Y. Bliokh, F. Nori, and J. Verbeeck, *Phys. Rev. Lett.* **110**, 093601 (2013).
- [6] T. Schachinger, S. L  ffler, M. St  ger-Pollach, and P. Schattschneider, *Ultramicroscopy* **158**, 17 (2015).
- [7] D. Sarenac, M. E. Henderson, H. Ekinci, C. W. Clark, D. G. Cory, L. DeBeer-Schmitt, M. G. Huber, C. Kapahi, and D. A. Pushin, *Sci. Adv.* **8**, eadd2002 (2022).
- [8] V. K. Ivanov, A. D. Chaikovskaia, and D. V. Karlovets, *Phys. Rev. A* **108**, 062803 (2023).
- [9] D. V. Karlovets, S. S. Baturin, G. Geloni, G. K. Sizykh, and V. G. Serbo, *Eur. Phys. J. C* **83**, 372 (2023).
- [10] L. Zou, P. Zhang, A. J. Silenko, and L. Lu, *Innovation* **4**, 100432 (2023).
- [11] K. Y. Bliokh and F. Nori, *Phys. Rep.* **592**, 1 (2015).
- [12] K. Y. Bliokh, *Phys. Rev. Lett.* **126**, 243601 (2021).
- [13] Y. Shen, X. Wang, Z. Xie, C. Min, X. Fu, Q. Liu, M. Gong, and X. Yuan, *Light Sci. Appl.* **8**, 90 (2019).
- [14] U. D. Jentschura and V. G. Serbo, *Phys. Rev. Lett.* **106**, 013001 (2011).
- [15] Z.-W. Lu, L. Guo, Z.-Z. Li, M. Ababekri, F.-Q. Chen, C. Fu, C. Lv, R. Xu, X. Kong, Y.-F. Niu, and J.-X. Li, *Phys. Rev. Lett.* **131**, 202502 (2023).

- [16] Y. Wu, S. Gargiulo, F. Carbone, C. H. Keitel, and A. Pálffy, *Phys. Rev. Lett.* **128**, 162501 (2022).
- [17] Y. Xu, D. L. Balabanski, V. Baran, C. Iorga, and C. Matei, *Phys. Lett. B* **852**, 138622 (2024).
- [18] A. Luski, Y. Segev, R. David, O. Bitton, H. Nadler, A. R. Barnea, A. Gorlach, O. Cheshnovsky, I. Kaminer, and E. Narevicius, *Science* **373**, 1105 (2021).
- [19] P. K. Maslennikov, A. V. Volotka, and S. S. Baturin, *Phys. Rev. A* **109**, 052805 (2024).
- [20] G. F. Quinteiro, F. Schmidt-Kaler, and C. T. Schmiegelow, *Phys. Rev. Lett.* **119**, 253203 (2017).
- [21] B. Mendis, *Ultramicroscopy* **239**, 113548 (2022).
- [22] G. F. Quinteiro Rosen, P. I. Tamborenea, and T. Kuhn, *Rev. Mod. Phys.* **94**, 035003 (2022).
- [23] A. J. Silenko, *Phys. Scr.* **99**, 025905 (2024).
- [24] F. Tamburini, F. Feleppa, I. Licata, and B. Thidé, *Phys. Rev. A* **104**, 013718 (2021).
- [25] M. Uchida and A. Tonomura, *Nature* **464**, 737 (2010).
- [26] J. Verbeeck, H. Tian, and P. ttschneider, *Nature* **467**, 301 (2010).
- [27] B. J. McMorran, A. Agrawal, I. M. Anderson, A. A. Herzog, H. J. Lezec, J. J. McClelland, and J. Unguris, *Science* **331**, 192 (2011).
- [28] K. Y. Bliokh, M. R. Dennis, and F. Nori, *Phys. Rev. Lett.* **107**, 174802 (2011).
- [29] I. Bialynicki-Birula and Z. Bialynicka-Birula, *Phys. Rev. Lett.* **118**, 114801 (2017).
- [30] S. M. Barnett, *Phys. Rev. Lett.* **118**, 114802 (2017).
- [31] K. Saitoh, Y. Hasegawa, K. Hirakawa, N. Tanaka, and M. Uchida, *Phys. Rev. Lett.* **111**, 074801 (2013).
- [32] V. Grillo, T. R. Harvey, F. Venturi, J. S. Pierce, R. Balboni, F. Bouchard, G. Carlo Gazzadi, S. Frabboni, A. H. Tavabi, Z.-A. Li, R. E. Dunin-Borkowski, R. W. Boyd, B. J. McMorran, and E. Karimi, *Nat. Commun.* **8**, 689 (2017).
- [33] A. Rajabi and J. Berakdar, *Phys. Rev. A* **95**, 063812 (2017).
- [34] K. van Kruining, A. G. Hayrapetyan, and J. B. Götze, *Phys. Rev. Lett.* **119**, 030401 (2017).
- [35] L. Zou, P. Zhang, and A. J. Silenko, *Phys. Rev. A* **103**, L010201 (2021).
- [36] C. Greenshields, R. L. Stamps, and S. Franke-Arnold, *New J. Phys.* **14**, 103040 (2012).
- [37] C. R. Greenshields, S. Franke-Arnold, and R. L. Stamps, *New J. Phys.* **17**, 093015 (2015).
- [38] G. M. Gallatin and B. McMorran, *Phys. Rev. A* **86**, 012701 (2012).
- [39] C. R. Greenshields, R. L. Stamps, S. Franke-Arnold, and S. M. Barnett, *Phys. Rev. Lett.* **113**, 240404 (2014).
- [40] D. Karlovets, *New J. Phys.* **23**, 033048 (2021).
- [41] A. J. Silenko, *Mod. Phys. Lett. A* **37**, 2250097 (2022).
- [42] L. L. Foldy and S. A. Wouthuysen, *Phys. Rev.* **78**, 29 (1950).
- [43] L. Zou, P. Zhang, and A. J. Silenko, *Phys. Rev. A* **101**, 032117 (2020).
- [44] G. K. Sizykh, A. D. Chaikovskaia, D. V. Grosman, I. I. Pavlov, and D. V. Karlovets, *Prog. Theor. Exp.* **2024**, 053A02 (2024).
- [45] L. Zou, P. Zhang, and A. J. Silenko, *J. Phys. G Nucl. Part. Phys.* **47**, 055003 (2020).
- [46] G. K. Sizykh, A. D. Chaikovskaia, D. V. Grosman, I. I. Pavlov, and D. V. Karlovets, *Phys. Rev. A* **109**, L040201 (2024).
- [47] M. Newstein and B. Rudman, *IEEE J. Quantum Electron.* **23**, 481 (1987).
- [48] S. Cruz y Cruz, Z. Gress, P. Jiménez-Macías, and O. Rosas-Ortiz, in *Geometric Methods in Physics XXXVIII* (Springer Cham, 2020).
- [49] M. Hiekkämäki, R. F. Barros, M. Ornigotti, and R. Fickler, *Nat. Photonics* **16**, 828 (2022).
- [50] A. Siegman, *Lasers* (University Science Books, 1986).
- [51] R. Ducharme and I. G. da Paz, *Phys. Rev. A* **92**, 023853 (2015).
- [52] H. M. Moya-Cessa, S. A. Hojman, F. A. Asenjo, and F. Soto-Eguibar, *Optik* **252**, 168468 (2022).
- [53] S. Feng and H. G. Winful, *Opt. Lett.* **26**, 485 (2001).
- [54] S. Brennecke, N. Eicke, and M. Lein, *Phys. Rev. Lett.* **124**, 153202 (2020).
- [55] X. Gu, M. Krenn, M. Erhard, and A. Zeilinger, *Phys. Rev. Lett.* **120**, 103601 (2018).
- [56] K. M. Case, *Phys. Rev.* **95**, 1323 (1954).
- [57] A. Melkani and S. J. van Enk, *Phys. Rev. Res.* **3**, 033060 (2021).
- [58] C. Cohen-Tannoudji, B. Diu, and F. Laloë, *Quantum Mechanics, Volume 3: Fermions, Bosons, Photons, Correlations, and Entanglement* (Wiley, 2019).
- [59] D. Zwillinger, V. Moll, I. Gradshteyn, and I. Ryzhik, eds., *Table of Integrals, Series, and Products (Eighth Edition)* (Academic Press, 2014).
- [60] J. Izaac and J. Wang, *Computational Quantum Mechanics* (Springer Cham, 2019).
- [61] T. Sasaki, H. Sawada, F. Hosokawa, Y. Sato, and K. Suenaga, *Ultramicroscopy* **145**, 50 (2014).
- [62] B. J. McMorran, A. Agrawal, P. A. Ercius, V. Grillo, A. A. Herzog, T. R. Harvey, M. Linck, and J. S. Pierce, *Phil. Trans. R. Soc. A* **375**, 20150434 (2017).